

Figure 3.22 Linear attenuation coefficient as a function of the energy for calcium (Ca), water, and the contrast agent iodine (I) in water (10 mg/ml). Note the K-edge discontinuity of I at 33.2 keV.

$$\begin{aligned} a_p &\approx K_p \frac{\rho}{A} Z^n, & n &\approx 4 \\ a_c &\approx K_C \frac{\rho}{A} Z \end{aligned} \quad (3.60)$$

where K_p and K_C are constants, ρ is the mass density, A the mass number, and Z the atomic number of the attenuating medium.¹³

Using Eq. 3.59 it can easily be shown that the attenuation coefficient of an arbitrary substance can be written as a linear combination of the attenuation coefficient of two selected materials (e.g., water and iodine[‡]) in the absence of K-edge discontinuities in the used energy range $[E_{\min}, E_{\max}]$ and provided that the attenuation properties of both basis materials are sufficiently different. Hence

$$\mu(E, x, y) = a_1(x, y) \cdot \mu_1(E) + a_2(x, y) \cdot \mu_2(E). \quad (3.61)$$

Substituting Eq. 3.61 in Eq. 3.4 for a spectrum with energy range $[E_{\min}, E_{\max}]$ yields

$$\begin{aligned} I_\theta(r) &= \int_{E_{\min}}^{E_{\max}} \sigma(E) e^{-\int_{L_{r,\theta}} \mu(E, x, y) ds} dE \\ &= \int_{E_{\min}}^{E_{\max}} \sigma(E) e^{-\int_{L_{r,\theta}} (a_1(x, y) \cdot \mu_1(E) + a_2(x, y) \cdot \mu_2(E)) ds} dE, \end{aligned} \quad (3.62)$$

where $L_{r,\theta}$ is the projection line. Defining $A_1(r, \theta)$ and $A_2(r, \theta)$ as

$$A_1(r, \theta) = \int_{L_{r,\theta}} a_1(x, y) ds$$

$$A_2(r, \theta) = \int_{L_{r,\theta}} a_2(x, y) ds. \quad (3.63)$$

Eq. 3.62 can be rewritten as

$$\begin{aligned} I_\theta(r) &= \int_{E_{\min}}^{E_{\max}} \sigma(E) e^{-(A_1(r,\theta) \cdot \mu_1(E) + A_2(r,\theta) \cdot \mu_2(E))} dE. \end{aligned} \quad (3.64)$$

$A_1(r, \theta)$ and $A_2(r, \theta)$ represent the equivalent thickness of the basis materials along ray $L_{r,\theta}$. In this equation $A_1(r, \theta)$ and $A_2(r, \theta)$ are unknown, but they can be retrieved. Indeed, it is sufficient to acquire two projections, each at a different energy with corresponding spectra, say σ_{LE} and σ_{HE} , to calculate $A_1(r, \theta)$ and $A_2(r, \theta)$ from the following system of two nonlinear equations

$$\begin{aligned} I_{LE}(r, \theta) &= \int_{E_{\min}}^{E_{\max}} \sigma_{LE}(E) e^{-(A_1(r,\theta) \cdot \mu_1(E) + A_2(r,\theta) \cdot \mu_2(E))} dE \\ I_{HE}(r, \theta) &= \int_{E_{\min}}^{E_{\max}} \sigma_{HE}(E) e^{-(A_1(r,\theta) \cdot \mu_1(E) + A_2(r,\theta) \cdot \mu_2(E))} dE. \end{aligned} \quad (3.65)$$

Various approaches exist to solve Eqs. 3.65. For example, the inverse relationship can be modeled by a second- or third-order polynomial. From the above equations it is clear that two different spectra σ_{LE} and σ_{HE} are sufficient in the absence of K-edge discontinuities in the used energy range $[E_{\min}, E_{\max}]$. Multi-energy CT then becomes dual-energy CT, which is the way it is clinically implemented today.

If more than two measurements and corresponding equations are available, an optimization strategy is required to solve the overdetermined system. This is, for example, the case when photon counting detectors can be used. More information on numerical optimization can be found in Nocedal and Wright.¹⁴

As soon as $A_1(r, \theta)$ and $A_2(r, \theta)$ are known for all (r, θ) , the unknown tissue-dependent coefficients $a_1(x, y)$ and $a_2(x, y)$ can simply be reconstructed by, for example, filtered backprojection (Figure 3.23). From these values monochromatic images at any

[‡] Iodine has a relatively low K-edge energy of 33.2 keV, which is too low to play a role in general-purpose CT. For dedicated CT operating at lower kV, such as breast CT or small animal CT, it cannot be neglected anymore.

14 J. Nocedal and S. Wright. *Numerical Optimization*, volume XXII of *Springer Series in Operations Research and Financial Engineering*. Springer, second edition, 2006.

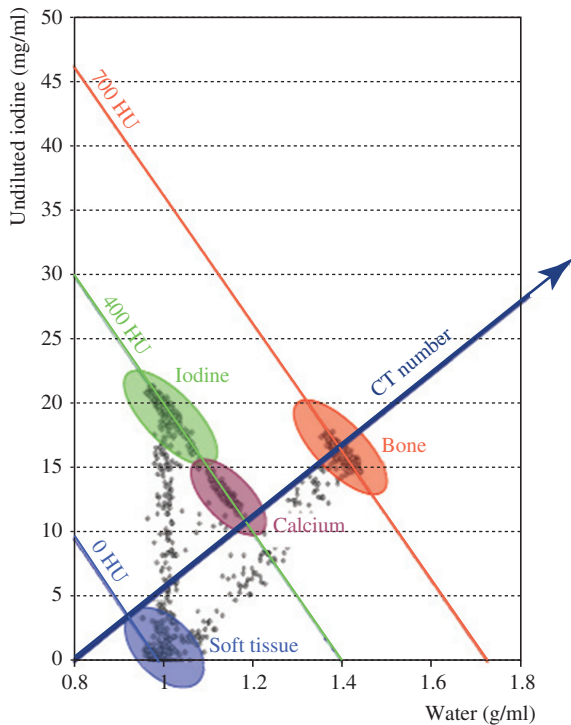


Figure 3.23 Using multi-energy imaging, each pixel can be represented as a linear combination of the attenuation coefficient of two basis materials. In conventional CT, different materials with the same average attenuation cannot be distinguished. In dual-energy imaging the material dependence of each tissue is characterized and therefore true tissue characterization can be performed. (Courtesy of GE Healthcare.)

energy (Figure 3.24(a)), images of the effective atomic numbers (Z_{eff} maps, Figure 3.24(b)), and single-substance images can be calculated, for which different methods can be found in the literature.¹⁵

Applications of multi-energy CT include:

- elimination of beam hardening artifacts,
- automatic segmentation, for example, automatic bone removal,
- retrospective generation of (virtual) monochromatic images at any possible energy,

15 B. J. Heismann, J. Leppert, and Stierstorfer K. Density and atomic number measurements with spectral xray attenuation method. *Journal of Applied Physics*, 94(3):2073–2079, August 2003.

A. Bonnin, P. Duvauchelle, V. Kaftandjian, and P. Ponard. Concept of effective atomic number and effective mass density in dual-energy x-ray computed tomography. *Nuclear Instruments and Methods in Physics Research B*, 318:223–231, 2014.

- tissue characterization,
- virtual unenhanced images. A multi-energy examination with contrast agent allows an image to be produced as if there were no contrast agent. It eliminates the need for two scans, i.e., a precontrast (unenhanced) and a postcontrast scan. This way CT perfusion (CTP) and CT angiography (CTA) no longer suffer from inter-scan motion artifacts.

Two important criteria for multi-energy CT are the energy separation and the co-registration. The measurements need to occur at very different effective energies. If they are too similar, the noise will be amplified. In this respect, the dual-layer solution is the least favorable and the photon-counting approach the most. For dynamic imaging, it is important that two measurements of the same projection line at different energies occur simultaneously. For this reason the detector-based methods and fast kV-switching are preferable, while the rotate-rotate and the dual-source methods are less favorable.

In the presence of a substance with an observable K-edge (e.g., iodine, gadolinium, gold, bismuth) in the energy range $[E_{\text{min}}, E_{\text{max}}]$ the above theory needs some modification. In that case Eqs. 3.59 and 3.61 have to be extended with a third component and corresponding coefficients a_K and a_3 respectively. This yields a third unknown A_3 in Eq. 3.64 and consequently requires a multi-energy approach with at least three different measurements.¹⁶ The original image is then separated into three instead of two basis images, the third being an image of the substance with K-edge. The strength of *K-edge imaging* is that the energy dependence of a material is very different around the K-edge, resulting in a high sensitivity for multi-energy imaging. This offers opportunities for multi-agent imaging and nanoparticle contrast agents and drugs. Photon counting CT is the most appropriate acquisition technique for K-edge imaging because it naturally offers more than two X-ray bins. The other spectra separating methods struggle with radiation dose inefficiency, limited temporal resolution, and technical complexity.

16 E. Roessl and R. Proksa. K-edge imaging in x-ray computed tomography using multi-bin photon counting detectors. *Physics in Medicine and Biology*, 52:4679–4696, 2007.

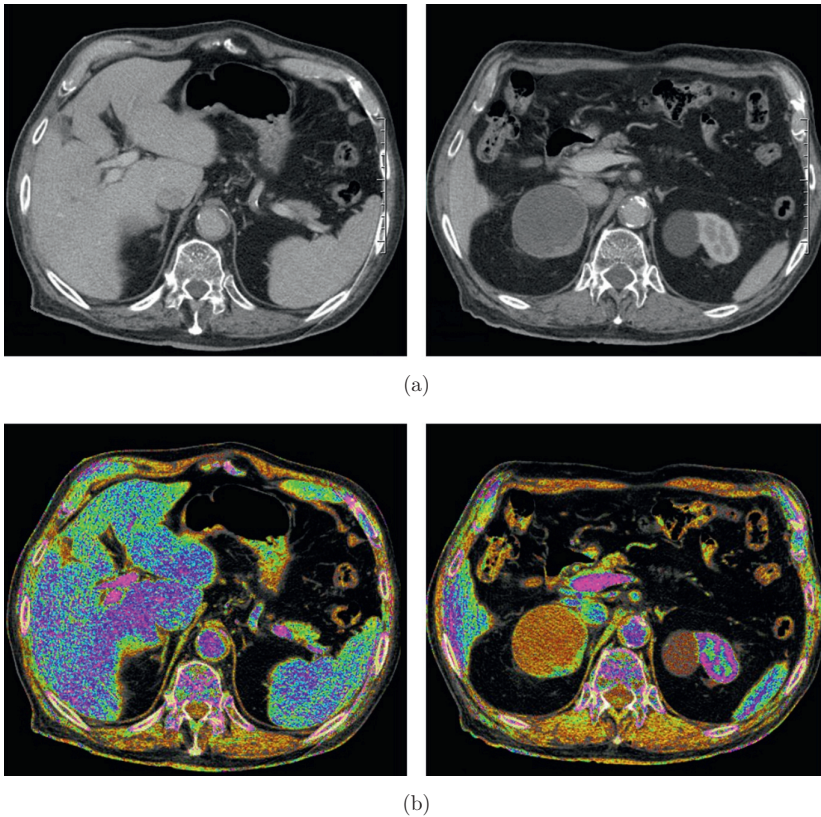


Figure 3.24 Results of the first abdominal studies with photon counting CT in 2008. **(a)** Monochromatic images at 70 keV. **(b)** Images of the effective atomic number (Z_{eff} maps). (Courtesy of GE Healthcare and Rabin Medical Center.)

3.6 Image Quality

3.6.1 Resolution

The spatial resolution in a CT image depends on a variety of factors.

- The size of the focal spot (see Section 2.5 p. 23).
- The size of the detector channels, as well as the amount of channel-to-channel crosstalk.
- The X-ray beam width is a combination of the above two factors. For locations closer to the focal spot, the focal spot size dominates the beam width. For locations closer to the detector, the detector cell size dominates the beam width.
- The continuous rotation of the tube-detector introduces a certain amount of azimuthal blur, which increases linearly with distance from the center of rotation. Hence, azimuthal blur can be significant at the periphery of the field-of-view.
- The reconstruction kernel or convolution filter, which can be tuned to enhance high frequencies for the sharpest images or to suppress

high frequencies for reduction of noise and aliasing.

- The interpolation process inherent to backprojection. This depends on the available sample density, which in turn depends on the channel size, the helical pitch, the detector quarter offset, and focal spot wobble or deflection.
- The voxel size. Normally, the voxel size is chosen smaller than the spatial resolution of the system, as defined by the above factors. Only if the voxel size is chosen larger, for example, to save computation time, does it become the bottleneck and determine the spatial resolution.

The in-plane spatial resolution in CT is typically defined as the value at which the MTF reaches a given percentage of its maximum. Current clinical CT scanners have an in-plane spatial resolution of about 15 lp/cm (at 10% MTF), depending on the reconstruction kernel. The effective slice thickness (FWHM of the SSP at the center of the field of view) can be as low as 0.5 mm.